Title: A peptide that regulates metalation of the *Arabidopsis* ethylene receptor

Authors: Anna J. Mudge[1]†, Saher Mehdi[1]††, Will Michaels[1,2]†, Beatriz Orosa-Puente[1]†††, Weiran Shen[1], Ari Sadanandom[1], Flora M. Hetherington[1], Claudia Hoppen[3], Buket Uzun[3], Georg Groth[3], Jennifer F. Topping[1], Nigel J. Robinson[1,2*], Keith Lindsey[1*]

Affiliations:
[1]*Department of Biosciences, Durham University, Durham, UK*
[2]*Department of Chemistry, Durham University, Durham, UK*
[3]*Institute of Biochemical Plant Physiology, Heinrich Heine University Düsseldorf, D-40204 Düsseldorf, Germany*

†These authors contributed equally to this work
††Present address: wellOwise Research and Development, IIITD Innovation & Incubation Centre, New Delhi, Delhi - 110020
†††Present address: School of Biological Sciences, University of Edinburgh, Edinburgh EH9 3FF, UK.
**Joint corresponding authors: keith.lindsey@durham.ac.uk; nigel.robinson@durham.ac.uk

Abstract: The vital plant ethylene receptor (ETR1) contains an essential Cu(I) ion, and as for other vesicular cupro-proteins, the final step of Cu(I) maturation at the endoplasmic reticulum (ER) is undefined. We previously discovered that mutants in the *Arabidopsis* gene *POLARIS* (*PLS*), encoding a 36 amino acid peptide, exhibit constitutive ethylene signalling responses. Here we report a 1:2 thiol-dependent Cu(I):PLS_2 complex, with an affinity of 3.79 (±1.5) x10^{19} M^{-2}. We demonstrate interactions with the transmembrane domain of ETR1, the Cu(I) chaperones ATX1 and CCH, and Cu(I)-transporting P_{1B}-type ATPase RAN1 at the ER. Formation of Cu(I)-dependent PLS-cuproprotein adducts at the ER provides a mechanism to modulate the metalation of ETR1, thereby regulating its activity and representing a distinct mechanism for plant hormone receptor regulation.

One Sentence Summary: The POLARIS peptide of Arabidopsis regulates activity of the ethylene hormone receptor by controlling Cu availability.

Main text: Ethylene is used by plants as a gaseous hormone to regulate many aspects of development and responses to biotic and abiotic stresses (*1*). It is perceived by a family of receptors that, in *Arabidopsis*, comprises 5 members, ETR1 (ETHYLENE RESPONSE 1), ERS1 (ETHYLENE RESPONSE SENSOR 1), ERS2, ETR2, and EIN4 (ETHYLENE-INSENSITIVE 4) (*2-5*) located on the endoplasmic reticulum (ER) (*6, 7*). The receptors are related to bacterial two-component systems (*2*), form dimers through disulphide bonding at the N-terminal hydrophobic domains (*8, 9*) and contain a Cu(I) ion bound to residues Cys65 and His69, essential for ethylene binding and signal transduction (*10, 11*). In the absence of ethylene these receptors activate a negative regulator CTR1 (CONSTITUTIVE TRIPLE RESPONSE 1), a mitogen-activated protein kinase kinase kinase (MAPKKK), so preventing ethylene responses (*12, 13*). Mechanisms by which receptor activity is regulated are not well understood. We describe here a molecular mechanism of the PLS peptide, and a proposed model for its role in plant development.

Introduction of copper to the ER and ethylene receptor requires the RAN1 (RESPONSIVE TO ANTAGONIST1) protein. This is a predicted copper-transporting P-type ATPase homologous to

the yeast Ccc2p and to human Menkes and Wilson disease proteins (*14*). Strong loss-of-function mutants of *RAN1* in *Arabidopsis* (e.g. *ran1-3*, *ran1-4*) exhibit a constitutive ethylene signalling response (*15*), consistent with a loss of receptor function, and similar to higher order loss-of-function receptor mutants, which also show an ethylene hypersignalling phenotype (*16*). Mechanisms of copper homeostasis, post-RAN1 but pre-ETR1, are unknown, and indeed this is true for other compartmentalized cuproproteins supplied with copper, for example via Ccc2p, Menkes or Wilson ATPases.

The *POLARIS* gene of *Arabidopsis* (AT4G39403) encodes a 36 amino acids peptide (Fig. 1A) that, in light-grown seedlings, is most strongly expressed in the root tip and vascular tissues (*17*). We have previously shown that the loss-of-function *pls* mutant is phenotypically similar to *ran1* loss-of-function alleles and *ctr1*, exhibiting a triple response phenotype (short hypocotyl and root, exaggerated apical hook, radial expansion) in the dark in the absence of ethylene (*18*), and a short root in light-grown seedlings (Fig. 1B). Transgenic complementation of the mutant and overexpression of the *PLS* gene suppresses the mutant phenotype, but fails to suppress the *ctr1* mutant phenotype, indicating that the PLS peptide acts upstream of CTR1 (*18*). The *pls* mutant phenotype is rescued by the gain-of-function ethylene resistant mutation *etr1-1* and pharmacological inhibition of ethylene signalling by silver ions (*18*). Ethylene gas production in the *pls* mutant is at wildtype levels, indicating the peptide plays a role in ethylene signalling rather than biosynthesis (*18*). RNA-seq on loss-of-function *pls* mutant and gain-of-function *PLS* transgenic overexpressor (PLSOx) seedlings shows that the *pls* mutant expresses no full length PLS coding sequence, while the PLSOx seedlings express ca. 18-fold higher levels of *PLS* transcript compared to wild-type (Fig. S1; Table S1). Gene Ontology (GO) analysis following RNA-seq transcriptomics of *pls* mutant seedlings shows the up-regulation of genes associated with responses to hormone signalling, biotic and abiotic defence responses, and cell death (Table S1; Fig. S2A). Eighty-four of 353 known ethylene-related genes are significantly up-regulated in the *pls* mutant compared to wildtype, and genes down-regulated in *pls* include categories associated with root morphogenesis, root epidermal cell differentiation, hormone biosynthetic processes, response to nutrients and metal ion transport (Fig. S2; *19*). In PLSOx overexpressors, up-regulated genes include those associated with hormone responses, biotic and abiotic stress responses and cell death; while 169 of 1615 genes associated with response to hormone stimulus are down-regulated compared to wildtype (Fig. S2C, D; *19*). Genes associated with metal ion transport are also down-regulated in PLSOx seedlings (Fig. S2D; *19*). Twenty-four ethylene-related genes are both up-regulated in the *pls* mutant and down-regulated in the PLS-overexpressor, compared with wild-type (Fig. 1C; *19*). This is consistent with a role for PLS in ethylene responses and other, potentially related, signalling, stress and developmental processes.

To further understand the relationship between PLS peptide structure and function, and to investigate conservation of PLS function between species, we carried out synthetic peptide feeding experiments using hydroponically grown seedlings. The *Arabidopsis* relative *Camelina sativa* contains a gene with partial sequence identity to the *Arabidopsis PLS* gene, encoding a predicted peptide sequence that is 22 amino acids long and identical to the N-terminal 22 amino acids of the *Arabidopsis* PLS except for a phenylalanine to serine substitution at position nine (Fig. 1A). We synthesized full-length PLS peptide, PLS(FL), and truncated versions from both *Arabidopsis* and *C. sativa* (Fig. 1A), and supplied the peptides to *Arabidopsis pls* mutant seedlings hydroponically. The full-length peptides from both *Arabidopsis* and *C. sativa* were each able to rescue the short primary root length of the *Arabidopsis pls* mutant (Fig. 1D), similar to transgenic overexpression and genetic complementation (*17, 18*). PLS(FL) peptide effects on root growth appear to be dose-dependent, as indicated both by genetic studies (*17*) and peptide feeding (Fig. S3A). However, neither a 9 amino acids sequence (N2, Fig. 1E) from the N-terminus, nor C-terminal sequences of

14 (C1) or 24 (C2) amino acids from *Arabidopsis* PLS were able to rescue the mutant (Fig. 1E). Imaging showed that a fluorescent tagged (5-carboxyfluorescein, 5-FAM) version of the *Arabidopsis* N-terminal 22 amino acids sequence of the peptide (N1) is taken up by the roots, and also rescues the mutant root phenotype (Fig. S3B, C).

Since genetic studies suggest that PLS acts close to the ethylene receptor (*18*), we hypothesized that it should localize to the same subcellular compartment. The ethylene receptor in *Arabidopsis* is localized to the ER (*12*), and ER localization of a proPLS::PLS:GFP fusion protein was confirmed by co-localization with the ER marker dye ER-Tracker™ (Fig. 2A-C) and with an ER-targeted red fluorescent protein RFP-HDEL (*20*) in transgenic plants (Fig. 2G-I). proPLS::PLS:GFP also appears to localize to the nucleus (Fig. 2). As controls, free GFP protein expressed under the control of the PLS promoter is not co-localized to the ER (Fig. 2D-F) and, as expected, the Golgi marker SH:GFP does not co-localize with ER Tracker (Fig. 2M-O). *Trans*-Golgi-localized SULFOTRANSFERASE1 (ST1) mCherry (*21*) show proPLS::PLS:GFP does not localize to the Golgi (Fig. 2J-L). To further clarify the side of the ER membrane on which PLS localizes, transient expression of redox-sensitive GFP (roGFP2) fusions of PLS were carried out. The different excitation properties of roGFP2 in an oxidizing (ER lumen) or reducing environment (cytosol) allows discrimination of the precise location of PLS. Ratiometric analysis and comparison with proteins of known localization revealed that PLS resides at the cytosolic side of the ER and is not localized in the ER lumen (Fig. 2P).

We hypothesized that PLS plays a role in receptor function and investigated whether this involved direct interaction with the receptor complex. Preliminary experiments using yeast 2-hybrid analysis suggested that PLS interacts with ETR1 (Fig. S4). Confirmation of the physical interaction between PLS and ETR1 in plants came from co-immunoprecipitation (Co-IP) analysis. *Agrobacterium* containing a plasmid encoding PLS linked to a C-terminal GFP and ETR1 with a C-terminal HA tag was infiltrated into *Nicotiana benthamiana* leaves for transient expression. After 3 d, interaction was confirmed by western blotting after Co-IP with either anti-GFP beads (showing PLS pulls down ETR1) or anti-HA beads (showing ETR1 pulls down PLS) (Fig. 3A). GFP-only controls did not show binding with ETR1, demonstrating the interaction is dependent on the presence of the PLS peptide.

The addition of 0.5 μM copper sulphate to the protein extract used for Co-IP experiments stabilized the PLS-ETR1 interaction. The presence of copper ions resulted in almost 3-fold more PLS:GFP detected upon pulldowns with ETR1-HA, or conversely of ETR1-HA pulled down with PLS-GFP, compared to the same assay in the presence of the metal chelator 2 mM EDTA (Fig. 3A,B).

To investigate the specificity of PLS binding, synthetic full length PLS peptide PLS(FL) was introduced into the infiltrated *N. benthamiana* leaves 30 min before the tissue was harvested. The addition of 25 nM synthetic PLS caused a ca. 80% reduction in PLS-GFP binding to ETR1-HA (Fig. 3C,D), suggesting that the synthetic PLS peptide competes for ETR1 binding, and showing the specificity of PLS for ETR1. Interestingly, the anti-GFP beads bound two sizes of PLS-GFP protein (Fig. 3E), both of which were larger than a GFP-only control, suggesting that the PLS peptide undergoes cleavage, a change in conformation, post-translational modification or incomplete reduction of Cys residues on some PLS. When using ETR1-HA to pull down PLS-GFP, only the larger peptide was present (Fig. 3E,F), suggesting that ETR1 binds the full length PLS peptide, but that PLS may be modified after ETR1 binding.

To pinpoint the interaction site at the receptor in more detail, binding studies were performed with purified receptor variants and PLS by microscale thermophoresis (MST; Fig. 3G). Binding of PLS was observed only with receptor variants containing the N-terminal transmembrane domain (TMD). In contrast, no binding was detected with ETR1 lacking this domain ($ETR1^{306-738}$). The

TMD harbors the ethylene and copper binding region (*22*).

Cysteine residues are common metal-ligand binding residues in low molecular weight copper-handling peptides, and predictions of PLS structure suggests a single α-helix plus unstructured region with two cysteines ($CX_{10}C$ arrangement where X is any amino acid), with some analogy to copper-metallochaperones such as Cox17 or other CX_9C twin proteins (*23*). In view of both structural considerations and the copper-dependency of ETR1 we determined whether the two cysteine residues (C6 and C17) in PLS play a functional role, such as in copper binding. A mutated *Arabidopsis* full-length peptide in which both cysteines were replaced with serine, PLS(FL C6S, C17S), was non-functional in root feeding assays (Fig. 4A), indicating the importance of the cysteine residues for biological activity. To determine a possible role for PLS in binding Cu(I), we first grew *pls* mutants and wildtype seedlings in the presence of the copper chelator bathocuproine disulphonic acid (BCS), which is often used to deplete copper but notably solubilises and stabilises Cu(I). Treatment of *pls* and wildtype seedlings with 10 μM and 50 μM BCS led to an increased primary root length of both genotypes, while 100 μM BCS led to significantly enhanced root growth in the *pls* mutant compared with wildtype (Fig. 4B); and rescue of the overexpression of ethylene-responsive genes (Fig. S5; *19*). This suggests that the availability of Cu(I) is growth-limiting in the *pls* mutant through abnormal ethylene perception.

Bicinchoninic acid (BCA) is a chromophore that binds Cu(I) (*24*) (Fig. 4C and S6). Titration experiments show that synthetic PLS(FL) withholds Cu(I) from BCA (Fig. S7), but the mutant PLS (FL C6S, C17S) does not (Fig. S8). Attempts to determine the stoichiometry and affinity for Cu(I) were confounded by precipitation of the synthetic peptide, whereas PLS fusion to maltose binding protein (MBP-PLS) retained solubility when titrated with Cu(I) ions under strictly anaerobic conditions. MBP-PLS (14 μM) withholds ca. 7 μM Cu(I) from BCA, indicative of a 2:1 PLS:Cu(I) stoichiometry, and tight binding is cysteine-dependent (Fig. 4D). A β_2 affinity of 3.79 (±1.5) $x10^{19}$ M^{-2} was determined by competition against an excess of BCA, and the fit significantly departs from simulations 10x tighter or weaker (Fig. 4E, Fig. S9).

Metal binding in biology is challenging to predict because the formation of metal-protein complexes is a combined function of metal affinity for a given protein and metal availability, which would need to be known for Cu(I) in the *Arabidopsis* cytosol in the case of PLS (Fig. 2P). Cu(I) occupancy of the cytosolic copper chaperone ANTIOXIDANT PROTEIN 1 (ATX1) tracks with fluctuations in available cytosolic Cu(I) such that its affinity approximates to the mid-point of the range of Cu(I) availabilities within this eukaryotic compartment (*25, 26*). *Arabidopsis* ATX1 was therefore expressed and purified to determine a 1:1 ATX1:Cu(I) stoichiometry and affinity $K_{D\ Cu(I)}$ of 5.47 (±0.6) $x10^{-18}$ M (Fig. 4F inset, Fig. S10). Figure 4F (main panel) reveals that the cytosolic concentration of PLS would need to exceed (improbable) millimolar concentrations for Cu(I)-dependent homodimers to form at this cytosolic Cu(I) availability (mathematical models and equations shown in Supplementary text). It is thus unlikely that the Cu(I):PLS_2 complex alone delivers Cu(I) to interacting cuproprotein ETR1. Cu(I)-dependent PLS heterodimeric adducts are the more likely functional species.

Together these results suggest a model in which PLS is involved in the RAN1-dependent maturation of Cu(I)ETR1 at the ER. To investigate possible interaction between PLS and RAN1, PLS was titrated to fluorescently labelled RAN1 and RAN1 truncation mutants. RAN1, NterRAN1 and CterRAN1 were purified and labelled as described (*27*). NterRAN1 is a truncation containing only the two N-terminal metal-binding-domains, whereas CterRAN1 is a construct lacking this region. Using Microscale Thermophoresis, direct interaction was observed between PLS and RAN1. Dissociation constants indicate that PLS interacts predominantly with the N-terminal metal-binding-domains, but only weakly with the C-terminal region (Fig. 4G). Moreover, the soluble copper chaperones ATX1 and CCH also interact with PLS. Titration experiments were

carried out with fluorescently labelled copper chaperones ATX, CCH and CCHΔ, a mutant lacking the plant specific C-terminal extension. PLS interacts with these soluble copper chaperones at similar affinity as obtained for RAN1 (Fig. 4H). Of relevance here is the observation that ATX1 interacts directly with RAN1 to deliver copper at the ER (*28*).
Cu(I)-dependent PLS heterodimeric adducts may therefore modulate multiple cuproproteins in the Cu(I)ETR1 maturation pathway.

The formation of PLS adducts with otherwise unsaturated copper coordination spheres, can inhibit the formation of aberrant copper-bridged complexes during metalation or during re-organisation of copper sites. This can, in turn, influence the rate of holo-ETR1 maturation, plus potentially the rates of ETR1 deactivation and reactivation. In this model, a down-regulation of *PLS* or loss-of-function mutation of the *PLS* gene leads to a depletion of correctly coordinated Cu(I) at the receptor through reduced intermediate PLS heterodimer adduct formation, in turn leading to a non-functional receptor that cannot activate CTR1, with a consequent activation of ethylene signaling, similar to *ran1* or *etr1* loss-of-function mutants, and/or through the effect of ethylene on reducing *PLS* expression (Figs. S11, S12). Overexpression of PLS phenocopies the ethylene-insensitive *etr1-1* gain-of-function mutant (*18*), presumably by a conformational change in the receptor on binding, to promote a functional interaction with CTR1 and suppressing ethylene responses. The PLS complex may be removed from ETR1 by dissociation of a PLS-ETR1-RAN1-chaperone complex following ligand-exchange, and/or modulated by PLS modification or cleavage. It is speculated that similar PLS-dependent events may also be required to re-set the receptor, perhaps following changes in the copper coordination sphere coincident with gain or loss of cation-π bonds between copper and ethylene. Hormonal regulation of *PLS* expression forms a signaling network to regulate ethylene responses and root growth with other hormones, such as by its activation to suppress growth-inhibitory ethylene responses in the high auxin environment of the root tip (*29*) (Fig. S12). Future structural studies should reveal more about the PLS-adduct-receptor interaction and role of copper ions in ethylene signal transduction, which represents a new paradigm for the regulation of signaling protein function by metals.

References

1. P.R Johnson, J.R. Ecker, The ethylene gas signal transduction pathway: A molecular perspective. *Ann. Rev. Genet.* ***32***, 227-254 (1998).

2. C. Chang, S.F. Kwok, A.B. Bleecker, E.M. Meyerowitz, Arabidopsis ethylene-response gene *ETR1* - similarity of product to 2-component regulators. *Science* **262**, 539-544 (1993).

3. J. Hua, C. Chang, Q. Sun, E.M. Meyerowitz, Ethylene insensitivity conferred by Arabidopsis *ERS* gene. *Science* **269**, 1712-1714 (1995).

4. J. Hua, H. Sakai, S. Nourizadeh, Q.G. Chen, A.B. Bleecker, J.R. Ecker, E.M. Meyerowitz, EIN4 and ERS2 are members of the putative ethylene receptor gene family in Arabidopsis. *Plant Cell* **10**, 1321-1332 (1998).

5. H. Sakai, J. Hua, Q.G. Chen, C. Chang, L.J. Medrano, A.B. Bleecker, E.M. Meyerowitz, *ETR2* is an *ETR1*-like gene involved in ethylene signaling in *Arabidopsis*. *Proc. Natl. Acad. Sci. USA* **95**, 5812-5817 (1998).

6. Y.F. Chen, M.D. Randlett, J.L. Findell, , G.E. Schaller, Localization of the ethylene receptor ETR1 to the endoplasmic reticulum of Arabidopsis. *J. Biol. Chem*. **277**, 19861-19866 (2002).

7. C. Grefen, K. Staedele, K. Ruzicka, P.Obrdlik, K. Harter, J. Horak, Subcellular localization and in vivo interactions of the *Arabidopsis thaliana* ethylene receptor family members. *Molec. Plant* **1**, 308-320 (2008).

8. G.E. Schaller, A.N. Ladd, M.B. Lanahan, J.M. Spanbauer, A.B. Bleecker, The ethylene response mediator ETR1 from Arabidopsis forms a disulfide-linked dimer. *J. Biol. Chem*. **270**, 12526-12530 (1995).

9. A.E. Hall, J.L. Findell, G.E. Schaller, E.C. Sisler, A.B. Bleecker, Ethylene perception by the ERS1 protein in Arabidopsis. *Plant Physiol.* **123**, 1449-1457 (2000).

10. F.I. Rodriguez, J.J. Esch, A.E. Hall, B.M. Binder, G.E. Schaller, A.B. Bleecker, A copper cofactor for the ethylene receptor ETR1 from Arabidopsis. *Science* **283**, 996-998 (1999).

11. B.K. McDaniel, B.M. Binder, ETHYLENE RECEPTOR 1 (ETR1) is sufficient and has the predominant role in mediating inhibition of ethylene responses by silver in *Arabidopsis thaliana*. *J. Biol. Chem.* **287**, 26094-26103 (2012).

12. C.R. Chang, Ethylene signaling: the MAPK module has finally landed. *Trends Plant Sci.* **8**, 365-368 (2003).

13. Z.Y. Gao, Y.-F. Chen, M.D. Randlett, X.-C. Zhao, J.L. Findell, J.J.Kieber, G.E. Schaller, Localization of the Raf-like kinase CTR1 to the endoplasmic reticulum of Arabidopsis through participation in ethylene receptor signaling complexes. *J. Biol. Chem*. **278**, 34725-34732 (2003).

14. T. Hirayama, J.J. Kieber, N. Hirayama, M. Kogan, P. Guzman, S. Nourizadek, J.M. Alonso, W.P. Dailey, A. Dancis, J.R. Ecker, RESPONSIVE-TO-ANTAGONIST1, a Menkes/Wilson disease-related copper transporter, is required for ethylene signaling in Arabidopsis. *Cell* **97**, 383-393 (1999).

15. B.M. Binder, F.I. Rodriguez, A.B Bleecker, The copper transporter RAN1 is essential for biogenesis of ethylene receptors in Arabidopsis. *J. Biol. Chem*. **285**, 37263-37270 (2010).

16. X. Qu, B.P. Hall, Z.Y. Gao, G.E. Schaller, A strong constitutive ethylene-response phenotype conferred on Arabidopsis plants containing null mutations in the ethylene receptors *ETR1* and *ERS1*. *BMC Plant Biol*. **7**, 3 (2007).

17. S.A. Casson, P.M. Chilley, J.F. Topping, I.M. Evans, M.A. Souter, K. Lindsey, The *POLARIS* gene of Arabidopsis encodes a predicted peptide required for correct root growth and leaf vascular patterning. *Plant Cell* **14**, 1705-1721 (2002).

18. P.M. Chilley, S.A. Casson, P.Tarkowski, N. Hawkins, K.L. Wang, P.J. Hussey, M. Beale, J.R. Ecker, G.K Sandberg, K. Lindsey, The POLARIS peptide of Arabidopsis regulates auxin transport and root growth via effects on ethylene signaling. *Plant Cell* **18**, 3058-3072 (2006).

19. A.J. Mudge, S. Mehdi, W. Michaels, B. Orosa-Puente, W. Shen, A. Sadanandom, F.M. Hetherington, C. Hoppen, B. Uzun, G. Groth, J.F. Topping, N.J. Robinson, K. Lindsey, Data from:

A peptide that regulates metalation of the *Arabidopsis* ethylene receptor. *Dryad Digital Repository.* https://doi.org/10.5061/dryad.wpzgmsbss.

20. H. Lee, I. Sparkes, S. Gattolin, N. Dzimitrowicz, L.M. Roberts, C. Hawes, L. Frigerio, An Arabidopsis reticulon and the atlastin homologue *RHD3-like2* act together in shaping the tubular endoplasmic reticulum. *New Phytol.* **197**, 481-489 (2013).

21. M. Bauer, J. Papenbrock, Identification and characterization of single-domain thiosulfate sulfurtransferases from Arabidopsis thaliana. *FEBS Lett*. **532**, 427-431 (2002).

22. S. Schott-Verdugo, L. Müller, E. Classen, H. Gohlke, G. Groth, Structural model of the ETR1 ethylene receptor transmembrane sensor domain. *Sci Rep.* **9,** 8869 (2019).

23. N.J. Robinson, D.R. Winge, Copper metallochaperones. *Ann. Rev. Biochem.* **79**, 537-562 (2010).

24. Z. Xiao, J. Brose, S., Schimo, S.M. Ackland, S. La Fontaine, A.G. Wedd, Unification of the copper(I) binding affinities of the metallo-chaperones Atx1, Atox1, and related proteins: detection probes and affinity standards. *J. Biol. Chem.* **286**, 11047-11055 (2011).

25. X. Morgan, M. T., Bourassa, D., Harankhedkar, S., McCallum, A. M., Zlatic, S. A., Calvo, J. S., … Fahrni, C. J., Ratiometric two-photon microscopy reveals attomolar copper buffering in normal and Menkes mutant cells. *Proc. Natl. Acad. Sci. USA* **116**, 12167–12172 (2019).

26. Y. Yu, C. H., Yang, N., Bothe, J., Tonelli, M., Nokhrin, S., Dolgova, N. V., … Dmitriev, O. Y., The metal chaperone Atox1 regulates the activity of the human copper transporter ATP7B by modulating domain dynamics. *J. Biol. Chem.* **292**, 18169 (2017).

27. C. Hoppen, L. Müller, S. Hänsch, B. Uzun, D. Milic, A.J. Meyer, S. Weidtkamp-Peters, G. Groth, Soluble and membrane-bound protein carrier mediate direct copper transport to the ethylene receptor family. *Sci Rep.* **9**, 10715 (2019).

28. W. Li, R.F. Lacey, Y Ye, J Lu, K.-C. Yeh, Y Xiao, L. Li, C.-K. Wen, B.M. Binder, Y Zhao, Triplin, a small molecule, reveals copper ion transport in ethylene signaling from ATX1 to RAN1. *PLOS Genet.* **13**, e1006703.

29. J. Liu, S. Mehdi, J. Topping, P. Tarkowski, K. Lindsey, Modelling and experimental analysis of hormonal crosstalk in Arabidopsis. *Molec. Systems Biol*. **6**, 373 (2010).

30. Y. Matsuzaki, M. Ogawa-Ohnishi, A. Mori, Y. Matsubayashi, Secreted peptide signals required for maintenance of root stem cell niche in Arabidopsis. *Science* **329**, 1065-1067 (2010).

31. S.J. Clough, A.F. Bent, Floral dip: a simplified method for *Agrobacterium*-mediated transformation of *Arabidopsis thaliana*. *Plant J*. **6**, 735-743 (1998).

32. H.L. Thompson, W. Shen, R. Matus, M. Kakkar, C. Jones, D. Dolan, S. Grellscheid, X.Yang, N. Zhang, S. Mozaffari-Jovin, C. Chen, X. Zhang, J.F. Topping, K. Lindsey, MERISTEM-DEFECTIVE regulates the balance between stemness and differentiaiton in the root meristem through RNA splicing control. *Development* **150**, dev201476.

33. M.I. Love, W. Huber, S. Anders, Moderated estimation of fold change and dispersion for RNA-seq data with DESeq2. *Genome Biol.* **15**, 550 (2014).

34. S. Zhong, Z. Lin, D. Grierson, Tomato ethylene receptor-CTR interactions: visualization of NEVER-RIPE interactions with multiple CTRs at the endoplasmic reticulum. *J. Exp. Bot.* **59**, 965-972 (2008).

35. F. Brandizzi, E.L. Snapp, A.G. Roberts, J. Lippincott-Schwartz, C. Hawes, Membrane protein transport between the endoplasmic reticulum and the golgi in tobacco leaves is energy dependent but cytoskeleton independent: Evidence from selective photobleaching. *Plant Cell* **14**, 1293-1309 (2002).

36. O. Voinnet, S. Rivas, P. Mestre, D. Baulcombe, An enhanced transient expression system in plants based on suppression of gene silencing by the p19 protein of tomato bushy stunt virus. *Plant J.* **33**, 949-956 (2003).

37. P. Kuzmič, DynaFit—A Software Package for Enzymology. *Meth. Enzymol*. **467**, 247–280 (2009).

Acknowledgements: We thank Prof. Steven Cobb (Durham University Department of Chemistry) for advice on peptide synthesis, and Dr. Andrew Foster (Durham University Department of Chemistry) for preliminary peptide-Cu interaction analysis.
Funding: The authors acknowledge financial support from:

UK Biotechnology and Biological Sciences Research Council BB/E006531/1, BBS/B/0773X, BB/J014516/1 (KL), BB/V006002/1, BB/M011186/1 (NJR).

Deutsche Forschungsgemeinschaft (German Research Foundation) 267205415 – SFB 1208 project B06 (GG).

Author contributions:
Conceptualization: KL, NJR, JFT
Methodology: KL, NJR, AS, GG
Investigation: AJM, SM, WM, BO-P, WS, FMH, CH, BU
Visualization: AJM, SM, WM, BO-P, WS, FMH, CH
Funding acquisition: KL, NJR, GG
Supervision: KL, JFT, NJR, AS, GG
Writing - original draft - KL, NJR, GG
Writing - review & editing - KL, NJR, GG, AS, AJM, SM, WM, BO-P, WS, FMH, CH, BU
Competing interests: Authors declare that they have no competing interests.

Data and materials availability: All data are available in the main text, supplementary materials and (for RNA-seq and root assay data) the Dryad Digital Repository (https://doi.org/10.5061/dryad.wpzgmsbss).

List of Supplementary Materials:
Materials and Methods
Supplementary Text
Figs. S1 to S12
Table S1

Figure Legends

Figure 1. The PLS peptide is required for ethylene control of seedling growth, is structurally and functionally conserved, and complements the *Arabidopsis pls* mutant.
(**A**). Amino acid sequence of the PLS peptide from *Arabidopsis thaliana* with *Camelina sativa* PLS sequence (*C.s* PLS), and synthetic truncations N1, N2, C1 and C2, indicated by horizontal lines. Two cysteine residues are highlighted in bold. (**B**) Wildtype (left) and *pls* mutant (right); bar = 5 mm. (**C**) Expression levels of 24 ethylene-responsive genes in *pls* and *PLS* overexpressing seedlings, compared to wildtype levels. (**D**) Effect of *Arabidopsis* PLS full length peptide, *A.t.* PLS(FL), and *Camelina* PLS peptide (*C.s.* PLS) on *Arabidopsis* primary root length. Wildtype (C24) and *pls* mutant seedlings were grown hydroponically in the presence (100 nM) or absence of peptide for 10 d. Asterisks: ANOVA, $F_{2, 41} = 6.86$, $p = 0.003$; Tukey's HSD test. (**E**) Effect of PLS full length and truncated peptides on *Arabidopsis* primary root length. Seedlings were grown hydroponically in the presence of 50 nM peptide for 10 d. C1 = C-terminal 14 amino acids, C2 = C-terminal 24 amino acids, N1 = N-terminal 22 amino acids, N2 = N-terminal 9 amino acids, full length PLS = 36 amino acids. Asterisks: ANOVA, $F_{5,112} = 6.13$, $p = 4.65E-5$). Error bars show ± 1 standard error.

Figure 2. PLS localizes to the endoplasmic reticulum.
(**A-O**) PLS::PLS:GFP fusion protein (**A, G, J**) colocalizes with endoplasmic reticulum markers ER Tracker (**B, C, C** inset) and RFP:HDEL (**H, I, I** inset), but free GFP does not (**D-F**, **M-O**). PLS:GFP staining is seen also in nuclei (n). PLS::PLS:GFP (**J**) does not co-localize with the *trans*-Golgi markers ST-mCherry SH:GFP (**K, L**). Scale bars = 25 µm (**C, L**), 10 µm (**F, I, O**). (**P**) Ratiometric analysis of roGFP2 fusion constructs transiently expressed in *N. benthamiana*. Comparison of excitation ratios of PLS-roGFP2 and roGFP2-PLS with control constructs (free roGFP, SEC22 fusions) reveals that PLS localizes to the cytosolic side of the ER.

Figure 3. PLS interacts with the ethylene receptor ETR1.
(**A**) Co-immunoprecipitation of PLS:GFP by ETR1:HA (upper panel) in leaves of *Nicotiana benthamiana*, in the presence and absence of 0.5 µM $CuSO_4$ and EDTA (to remove Cu). Lower panel shows presence of ETR1:HA in extracts using anti-HA antibody. (**B**) Densitometric scan of immunoblot. (**C**) Competition assay showing a reduced binding between PLS:GFP and ETR1:HA in the presence of 0, 5 nM or 25 nM PLS peptide, in the presence of 0.5 µM $CuSO_4$ and 50 µM MG-132, a proteasome inhibitor (upper panel). Lower panel shows ETR1:HA in extracts using anti-HA antibody. (**D**) Densitometric scan of immunoblot. (**E**) Co-immunopreciptation of ETR1:HA (upper panel) in leaves of *N. benthamiana*, showing the effect of EDTA (to remove Cu) on interaction between ERT1:HA and PLS:GFP. Lower panel shows presence of ETR1:HA in extracts using anti-HA antibody (**F**) Densitometric scan of immunoblot. α-GFP, anti-GFP antibody; α-HA, anti-HA antibody. (**G**) Microscale thermophoresis binding curves of different ETR1 truncations with PLS. Binding of PLS was observed with full-length ETR1 and all C-terminal truncations but not with $ETR1^{306-738}$ lacking the N-terminal transmembrane part of the receptor.

Figure 4. PLS binds copper and interacts with RAN1 and copper chaperones.
(**A**) C6S and C17S in PLS are required for function. Seedlings were grown hydroponically for 10 d in the presence (100 nM) or absence of peptide (FL or C6S, C17S). Asterisk: ANOVA, $F_{2, 51} = 9.48$, $p = 3.15E-4$, Tukey's HSD). Error bars show ± 1 standard error. Blue bars are C24, red bars are *pls*. (**B**) Effect of exogenous Cu(I) chelator BCS on primary root length of *Arabidopsis* grown hydroponically for 10 d. Asterisks: Student's t test analysis, $p < 0.005$. Error bars show ±1 standard error. (**C**) Absorption of BCA (17.3 µM) titrated with Cu(I) (representative spectrum, n=2, full dataset Fig S1). (**D**) Binding isotherms ($A_{358\ nm}$) of BCA (10 µM) in the presence/absence (filled/empty symbols, respectively) of 14 µM MBP-PLS (circles) or MBP-PLS mutants (C6S, C17S and C6S/C17S: triangles, diamonds and squares respectively) titrated with Cu(I) (n=3, ±SD). (**E**) Binding isotherms ($A_{358\ nm}$) of BCA (50 µM) in the presence/absence of 10 µM MBP-PLS (filled/empty symbols, respectively) titrated with Cu(I). Model (solid line) describes Cu(I)-binding as a 2:1 complex, with β_2 affinity of 3.79 (±1.5) $x10^{19}$ M^{-2}. Dotted lines simulate 10x weaker or tighter affinity (n=3, ±SD). (**F**) Simulated Cu(I) occupancy (Supplementary Text) as a function of [PLS] using β_2 Cu(I) affinity of 3.79 $x10^{19}$ M^{-2}. Inset, *Arabidopsis* ATX1 (20 µM, filled circles) withholds one Cu(I) equivalent from 20 µM BCA (open circles, BCA-alone) (n=3, ±SD), with K_D Cu(I) 5.47 $x10^{-18}$ M (Fig. S3). (**G**) Microscale thermophoresis binding curves of copper transporter RAN1 with PLS. (**H**) Microscale thermophoresis binding curves of soluble copper chaperones ATX1 and CCH with PLS.

Fig. 1

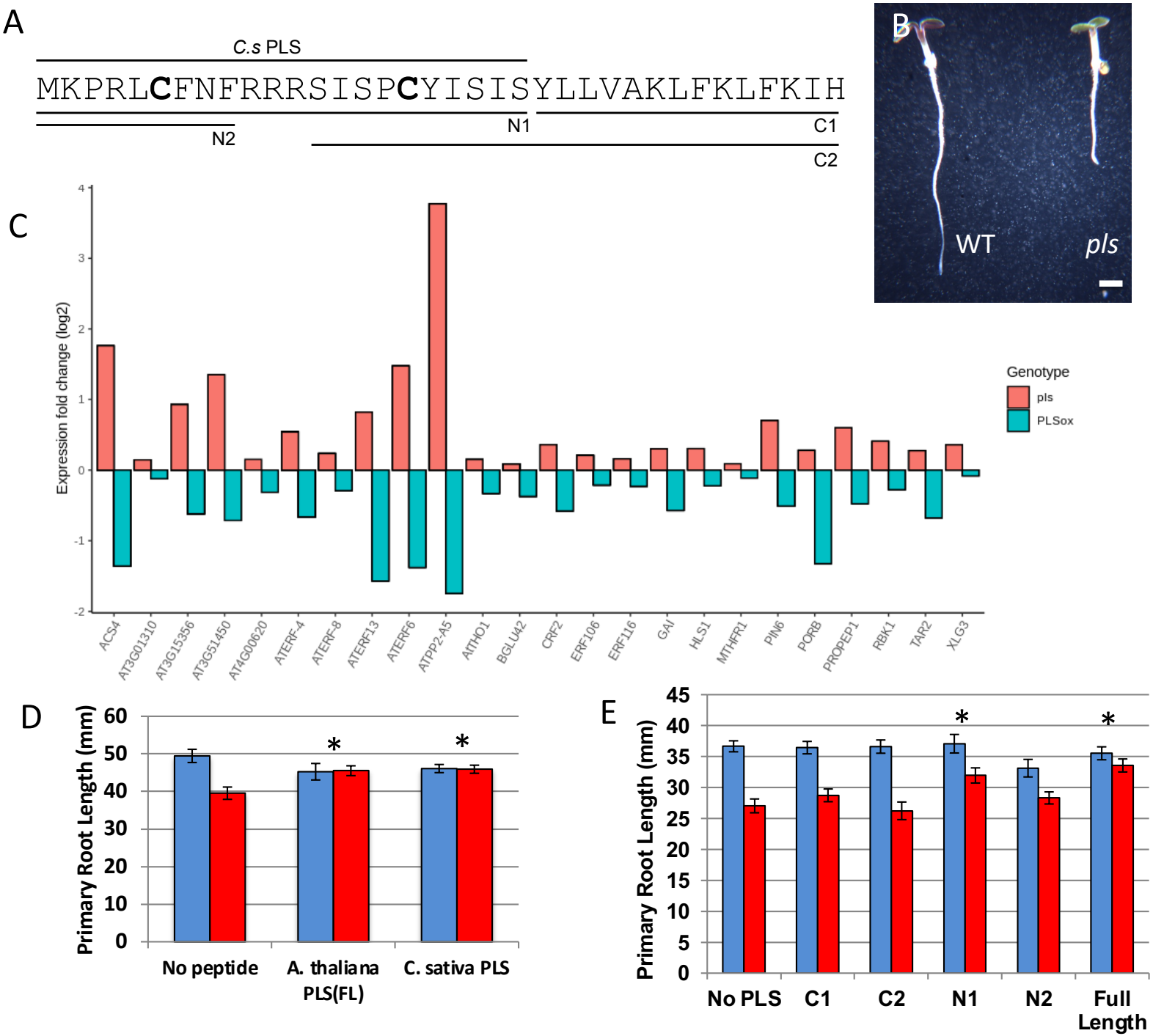
A
C.s PLS
MKPRLCFNFRRRSISPCYISISYLLVAKLFKLFKIH
N2
N1
C1
C2
B
WT
pls
C
Expression fold change (log2)
Genotype
pls
PLSox
ACS4
AT3G01310
AT3G15356
AT3G51450
AT4G00620
ATERF-4
ATERF-8
ATERF13
ATERF6
ATPP2-A5
ATHO1
BGLU42
CRF2
ERF106
ERF116
GAI
HLS1
MTHFR1
PIN6
PORB
PROPEP1
RBK1
TAR2
XLG3
D
Primary Root Length (mm)
No peptide
A. thaliana PLS(FL)
C. sativa PLS
E
Primary Root Length (mm)
No PLS
C1
C2
N1
N2
Full Length

Fig. 2

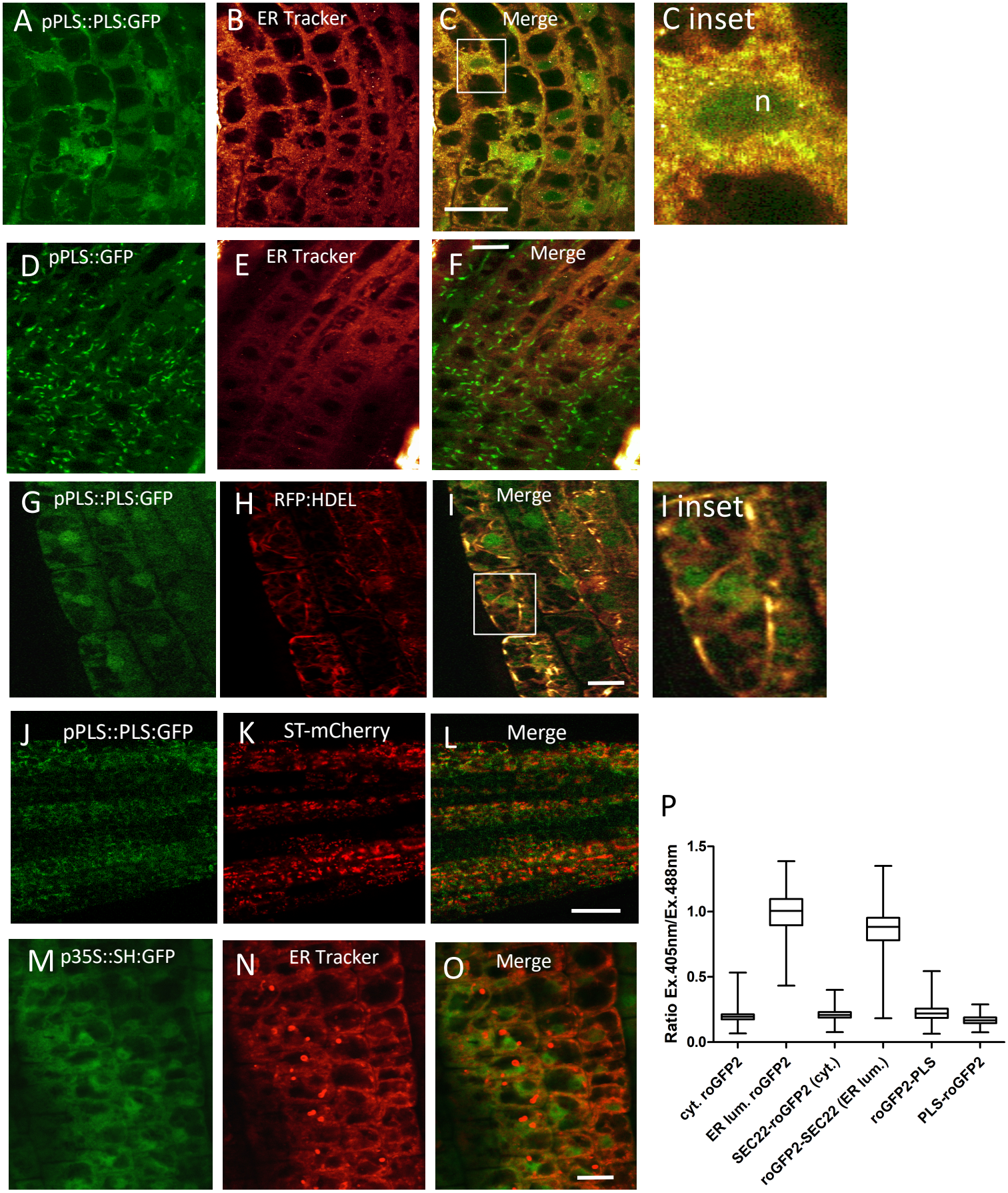
A pPLS::PLS:GFP
B ER Tracker
C Merge
C inset
n
D pPLS::GFP
E ER Tracker
F Merge
G pPLS::PLS:GFP
H RFP:HDEL
I Merge
I inset
J pPLS::PLS:GFP
K ST-mCherry
L Merge
M p35S::SH:GFP
N ER Tracker
O Merge
P
Ratio Ex.405nm/Ex.488nm
1.5
1.0
0.5
0.0
cyt. roGFP2
ER lum. roGFP2
SEC22-roGFP2 (cyt.)
roGFP2-SEC22 (ER lum.)
roGFP2-PLS
PLS-roGFP2

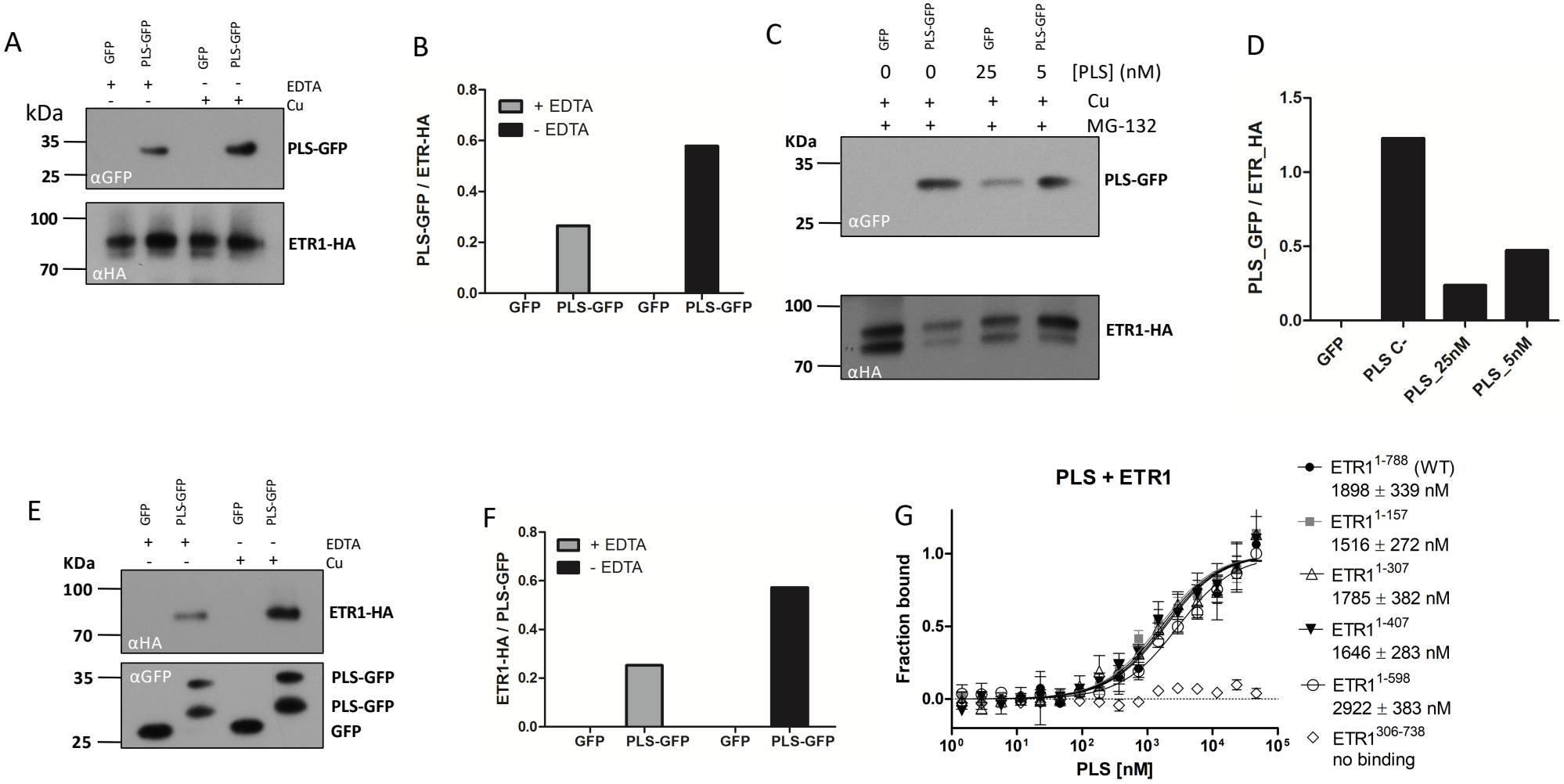
A
GFP
PLS-GFP
GFP
PLS-GFP
EDTA
Cu
kDa
35
25
αGFP
PLS-GFP
100
70
αHA
ETR1-HA
B
+ EDTA
- EDTA
PLS-GFP / ETR-HA
0.8
0.6
0.4
0.2
0.0
GFP
PLS-GFP
GFP
PLS-GFP
C
GFP
PLS-GFP
GFP
PLS-GFP
0
0
25
5
[PLS] (nM)
Cu
MG-132
KDa
35
25
αGFP
PLS-GFP
100
70
αHA
ETR1-HA
D
PLS_GFP / ETR_HA
1.5
1.0
0.5
0.0
GFP
PLS C-
PLS_25nM
PLS_5nM
E
GFP
PLS-GFP
GFP
PLS-GFP
EDTA
Cu
KDa
100
70
αHA
ETR1-HA
35
25
αGFP
PLS-GFP
PLS-GFP
GFP
F
+ EDTA
- EDTA
ETR1-HA / PLS-GFP
0.8
0.6
0.4
0.2
0.0
GFP
PLS-GFP
GFP
PLS-GFP
G
PLS + ETR1
Fraction bound
1.0
0.5
0.0
PLS [nM]
ETR1 1-788 (WT)
1898 ± 339 nM
ETR1 1-157
1516 ± 272 nM
ETR1 1-307
1785 ± 382 nM
ETR1 1-407
1646 ± 283 nM
ETR1 1-598
2922 ± 383 nM
ETR1 306-738
no binding

Fig. 3

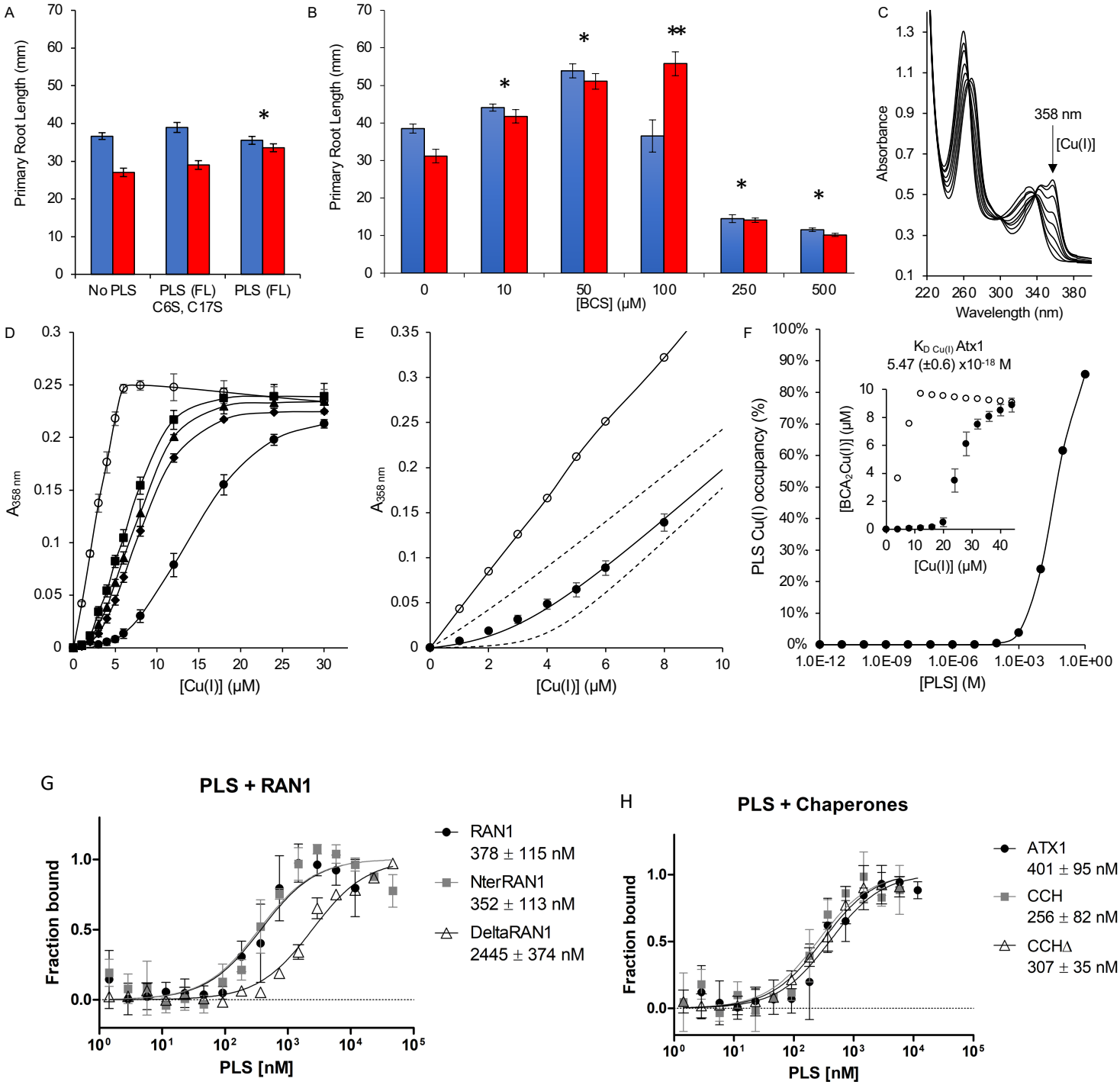
A
Primary Root Length (mm)
No PLS
PLS (FL) C6S, C17S
PLS (FL)
B
Primary Root Length (mm)
[BCS] (μM)
C
Absorbance
358 nm
[Cu(I)]
Wavelength (nm)
D
A358 nm
[Cu(I)] (μM)
E
A358 nm
[Cu(I)] (μM)
F
PLS Cu(I) occupancy (%)
[PLS] (M)
K D Cu(I) Atx1
5.47 (±0.6) x10-18 M
[BCA2Cu(I)] (μM)
[Cu(I)] (μM)
G
PLS + RAN1
Fraction bound
PLS [nM]
RAN1
378 ± 115 nM
NterRAN1
352 ± 113 nM
DeltaRAN1
2445 ± 374 nM
H
PLS + Chaperones
Fraction bound
PLS [nM]
ATX1
401 ± 95 nM
CCH
256 ± 82 nM
CCHΔ
307 ± 35 nM

Fig. 4